Med Biol Eng Comput (2012) 50:947–959
DOI 10.1007/s11517-012-0937-1

ORIGINAL ARTICLE

A model of tissue differentiation and bone remodelling in fractured vertebrae treated with minimally invasive percutaneous fixation

A. Boccaccio · D. J. Kelly · C. Pappalettere

Received: 10 January 2012 / Accepted: 13 June 2012 / Published online: 30 June 2012

Abstract In spite of the consolidated clinical use of minimally invasive percutaneous fixation techniques, little is reported in the literature providing a mechanobiological explanation for how the design of fixation devices can affect the healing process within fractured vertebrae. The aim of this study was to develop a multi-scale mechano-regulation model capable of predicting how the patterns of tissue differentiation within a vertebral fracture change in the presence or in the absence of fixation devices and how the dimensions of the device, and the materials it is made from (Ti-6Al-4V alloy and cobalt chrome alloy) can affect the outcome of the healing process. The macro-scale model simulates the spinal segment L3-L4-L5, including the fractured body of the L4 vertebra, while the micro-scale model represents a fractured portion of cancellous bone. The macro-scale model also includes a minimally invasive percutaneous fixation device. The model predicts that fixation devices significantly shorten healing times. Increasing values of the rod diameter D and decreasing values of its radius of curvature R lead to shorter durations of the healing period. Manufacturing the rods in cobalt chrome alloy is also predicted to reduce slightly the healing period by providing greater mechanical stability within the fracture callus.

Keywords Mechanobiology · Minimally invasive percutaneous fixation · Spine · Vertebral fracture · Tissue differentiation

1 Introduction

Many vertebral compression fractures without neurological involvement can be safely treated in a conservative way [25, 36]. Numerous studies have demonstrated the successful application of conservative treatments for some vertebral fractures, for example bed rest followed by external orthesis, exercise in extension, etc. [4, 12, 25, 34, 37, 39, 40]. Apart from the specific adopted methodology, the treatment should continue for at least 3/4 months during which the compliance and the collaboration of the patient are of crucial relevance. The problems related to an excessively long bed rest period are numerous and it can be very difficult to quantify them [28]. In case of polytrauma, claustrophobia, psychological disease, venous disease or previous deep venous thrombosis, obesity and broncho-pulmonary diseases, conservative treatment is not a viable treatment option. Moreover, conservative treatments expose the patient to higher risks of spinal deformity; for instance, the vertebral body wedging could lead to progressive spinal disorders such as kyphosis [27] that can consistently worsen the patient's quality of life. On the other hand, treating a vertebral fracture (that could be submitted to a conservative treatment) with a traditional

Electronic supplementary material The online version of this article (doi:10.1007/s11517-012-0937-1) contains supplementary material, which is available to authorized users.

A. Boccaccio (✉) · C. Pappalettere
Dipartimento di Ingegneria Meccanica e Gestionale, Politecnico di Bari, Bari, Italy
e-mail: a.boccaccio@poliba.it

A. Boccaccio
Società Cooperativa Sociale e Sanitaria: ONLUS "Insieme con Padre Pio", Martina Franca, Italy

D. J. Kelly
Trinity Centre for Bioengineering, Trinity College Dublin, Dublin, Ireland

open surgery may be an overtreatment considering the typical possible surgical complications (e.g. excessive blood loss, problems correlated with the anaesthesia, etc.). In such a context, a good compromise may be the percutaneous minimally invasive fixation surgery. This technique can be used every time when a conservative treatment cannot be applied or is not advisable and a posterior open arthrodesis may represent an overtreatment. The minimally invasive percutaneous fixation (MIPF) leads to clinical and functional results that are better or comparable to those obtained with a conservative treatment; time of recovery is quicker and the rate of complications is low [3, 27].

Mechanical factors are known to play a key role in bone fracture healing [13, 29]. Different numerical models have been proposed which relate the tissue differentiation process occurring during healing of long and flat bones and osteochondral defects to the mechanical environment within the mesenchymal tissue [5, 6, 8, 10, 14, 17, 19, 21, 23]. Recently, more sophisticated mechano-regulation models have been developed that include factors such as random-walk algorithms of cell dispersal [31], angiogenesis [11, 16, 30], cell-phenotype specific activity [20] and the role of the mechanical environment on the collagen architecture in regenerating soft tissues [26]. Using the mechanobiological model [14] and fuzzy rules adapted from previous studies [1, 38], Shefelbine et al. [35] demonstrated that the mechano-regulation principles regulating the healing process of diaphyseal fractures hold in case of fracture repair within trabecular bone.

In a previous study [9], a multi-scale mechano-regulation model was developed simulating the healing process occurring within the trabecular bone of a wedge vertebral fracture. The model successfully predicted the patterns of tissue differentiation during the healing process at the level of the individual trabeculae during the first 100 days after the fracture event. In the present study, we expanded this model to include the effect of minimally invasive percutaneous fixation devices (MIPFD). The objectives of the study are to evaluate: (i) how the spatial and temporal patterns of tissue differentiation change in the presence or in the absence of a MIPFD; (ii) how these patterns change for different geometrical parameters of MIPFD or for different materials with which such devices can be fabricated and (iii) the von Mises stress distribution within the MIPFD towards the end of the healing phase to quantify the risk of a possible failure of the stabilisation device and to understand whether or not its removal is required. Our hypothesis is that the presence of fixation devices decreases the overall level of the biophysical stimulus acting on the mesenchymal tissue, leading to a prediction of a reduced soft tissue formation and accelerated bone repair.

2 Methods

2.1 Macro-scale model of the spinal segment

Two different finite element models of the spinal segment L3-L4-L5 were created (Fig. 1). The first one includes the fractured body of the L4 vertebra (Fig. 1a), the second one, in addition to the fractured vertebra, includes the model of a minimally invasive fixation device (Fig. 1b). The finite element code ABAQUS was utilised. CT scan data have been utilised for the generation of the finite element mesh of the entire L3 and L5 vertebrae and the posterior processes of the L4 vertebra. A simplified model of the body of the L4 vertebra as well as the intervertebral discs located

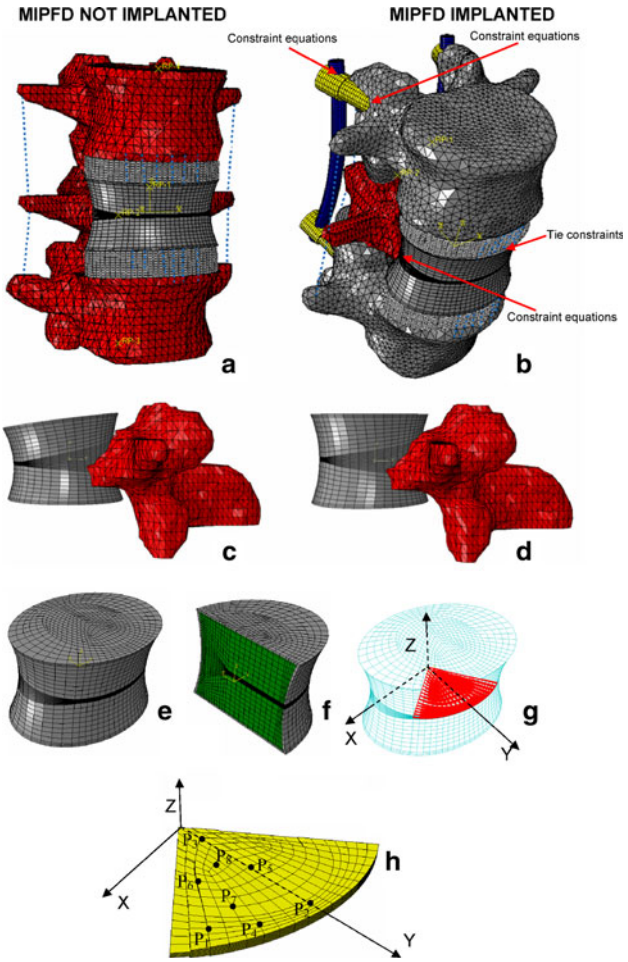

Fig. 1 Finite element model of the spinal segment L3-L4-L5 in the case of fixation devices absent (**a**) and present (**b**). The height of the fractured vertebra L4 was assumed to decrease from the posterior processes towards the anterior side in the case of MIPFD absent **c** and to remain constant in the case of MIPFD present **d**. The body of the L4 includes the cortical shell (*in gray*, **e**) the cancellous bone (*in green*, **f**) and the fracture gap [*highlighted in red* **g** and represented as isolated (*in yellow*) **h**]. The points P_1, P_2, …, P_8 within the fracture gap in correspondence of which the analysis of the fracture repair process was carried out are indicated (colour figure online)

above and below was developed in CAD environment. The models comprised of parts modelled as deformable [i.e.: in the case of MIPFD absent, the body of the L4 vertebra (gray); in the case of MIPFD present, the L3, L5 vertebrae (gray), the body of L4 (gray), the screws (yellow) and the rods (blue), Fig. 1a, b] and parts modelled as rigid bodies [i.e.: in the case of MIPFD absent, the L3, L5 vertebrae (red) and the posterior processes of the L4 (red); in the case of MIPFD present, the posterior processes of the L4 vertebra (red), Fig. 1a, b]. The strategy of modelling some parts of the spinal segment as un-deformable rigid bodies was adopted to reduce the computational cost of the analyses. In the case where fixation devices are not implanted, the vertebral height of the L4 decreases by the 20 % from the posterior processes towards the anterior side (Fig. 1c). In the case where a MIPFD is implanted, following the assumption that a complete reduction of the vertebral fracture was obtained (i.e. the fractured vertebra recovers its original height) after preliminary surgical treatment, the height of the fractured L4 vertebra was modelled as constant (Fig. 1d). Between the intervertebral discs and the vertebral bodies a 'tie' constraint was applied (Fig. 1b); constraint equations were used at the interfaces bone/screw, posterior processes/L4 body, rod/screw (Fig. 1b).

The body of the fractured L4 includes the cortical shell with a thickness of 0.5 mm [24], the cancellous bone and the fracture gap (Fig. 1e–h). The cancellous and the cortical bone have been modelled as biphasic poroelastic materials possessing transversely isotropic elastic properties. The spatial distribution of the cancellous bone Young's modulus was assumed to be heterogeneous. The L3 and L5 vertebrae include the cortical shell 0.5 mm thick and the cancellous bone. Also, in this case these tissues have been assumed to possess transversely isotropic properties and the cancellous bone to possess mechanical properties heterogeneously distributed in the space (Fig. ESM_1 available online (ESM_1.pdf)). Further details regarding the values of the mechanical properties utilised for the cancellous and cortical bone as well as the user-defined FORTRAN subroutine utilised to model the heterogeneous distribution of cancellous bone material properties are reported [9].

Each intervertebral disc includes the cartilagineous endplates, the nucleus polposus, and the annulus fibrosus with the collagen fibres. The flavum, intertransverse, interspinous and supraspinous ligaments have been included in the model. Further details about the modelling of the intervertebral discs and of the ligaments are reported [7, 9].

The minimally invasive percutaneous fixation devices include two principal components: the screws and the rods. Different dimensions for each component have been modelled in this study (Fig. 2a). The screw diameters D_S available on the market come in the following dimensions:

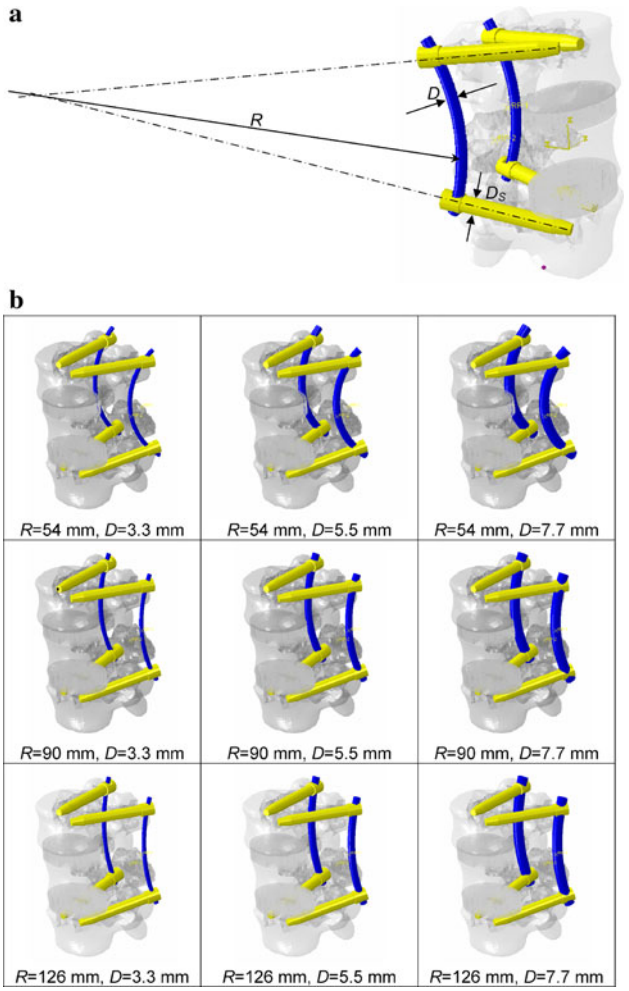

Fig. 2 **a** Geometrical parameters investigated. Three different values have been hypothesised for the rod diameter D and for the radius of curvature R. The sensitivity of the fracture healing process to the screw diameters D_S appears to be of negligible entity. **b** Schematic of the $3 \times 3 = 9$ cycles of analyses performed for each material hypothesised for the rod elements

4.5, 5.5, 6.5, 7.5 and 8.5 mm. Preliminary finite element analyses revealed that very small differences can be seen between the patterns of tissue differentiation predicted by the proposed model for different screw diameters. In other words, the sensitivity of the fracture healing process to the screw diameters D_S appears practically negligible. All the simulations presented in the manuscript refer to the case $D_S = 8.5$ mm. The rod diameter D had a more dramatic effect (Fig. 2a). The typical value of D for devices available on the market is $D = 5.5$ mm. The proposed mechano-regulation model has been utilised to predict how the patterns of tissue differentiation change if the diameter D increases or decreases by 40 %. Hence, three different values have been hypothesised for the rod diameter: $D = 5.5$ mm, $D = 5.5 \times 1.4 = 7.7$ mm and $D = 5.5 \times 0.6 = 3.3$ mm. Another important geometrical parameter

for the rod is the radius of curvature R (Fig. 2a). The radius of curvature R is typically $R = 90$ mm. As in the case of the rod diameter, three different radii of curvature have been considered in the present study: $R = 90$ mm, $R = 90 \times 1.4 = 126$ mm and $R = 90 \times 0.6 = 54$ mm. (Note: 40 % is a threshold value, if the radius of curvature decreases by more than 40 %, the rod model penetrates within the body of the L4 vertebra). A total of $3 \times 3 = 9$ analyses have been performed with the different hypothesised values of D and R according to the schematic shown in Fig. 2b.

The material of which the screws are typically realised is the Ti-6Al-4V alloy ($E = 110{,}000$ MPa, $v = 0.3$) while the rods are realised both, in Ti-6Al-4V alloy or, very recently, in cobalt chrome alloy ($E = 230{,}000$ MPa, $v = 0.3$). In summary, in the case of MIPFD implanted, 18 cycles of analysis have been performed, 9 for the case of rods in Ti-6Al-4V alloy and 9 for the case of rods in cobalt chrome alloy. In the case of MIPFD absent, just one cycle of analysis has been run.

2.2 Micro-scale model of trabecular bone

The micro-scale model of the trabecular bone is the same as that utilised by Shefelbine et al. [35] (Fig. 3). Prismatic domains 0.1 mm thick portrayed the trabeculae bordering the gap. The space between fractured trabeculae was hypothesised to be 0.5 mm high, according to the model of Shefelbine et al. [35], and occupied by granulation tissue. Both the trabecular bone and the granulation tissue were modelled as biphasic poroelastic materials. Further details about the micro-scale finite element model of trabecular bone are reported [9].

2.3 Multi-scale mechano-regulation model of tissue differentiation

A multi-scale approach was adopted [9]. The equations describing tissue differentiation were implemented into an algorithm, a graphical summary of which is depicted in Fig. 4. The time period investigated corresponds to the first 100 days after the fracture event. The macro-scale model of the spinal segment with and without MIPFD was utilised to determine the elastic and poroelastic boundary conditions acting on eight different micro-scale models which were hypothesised to represent different regions in the fractured cancellous bone located in the neighbourhood of the points P_1, …, P_8 (Fig. 1h). In order to evaluate the above-mentioned boundary conditions, an axial compression of 1,000 N—which is the typical load acting on the lumbar vertebrae of a 70 kg subject in the erect standing position—was applied in the centre of mass of the L3 vertebra and ramped over a time period of 1 s (which can be considered the time in which a subject assumes the erect position). The nodes located on the inferior surface of the L5 vertebra have been clamped (Fig. 4, Block{1}, {2}, {3}, {3bis} {4}). To switch from the macro to the micro-scale model, proper localization rules have been utilised (Fig. 4, Block{5}). A group of about 10 elements situated in the neighbourhood of each point P_1, …, P_8 within the macro-scale model is considered; for each group, the average value of strain in the vertical direction ε_{zzPi}, and pore pressure p_{pore} are determined. The micro-scale model, in turn, served to predict the local patterns of the tissues differentiating during the fracture repair process. A compression test was simulated on the micro-scale model reproducing the same elastic and poroelastic boundary

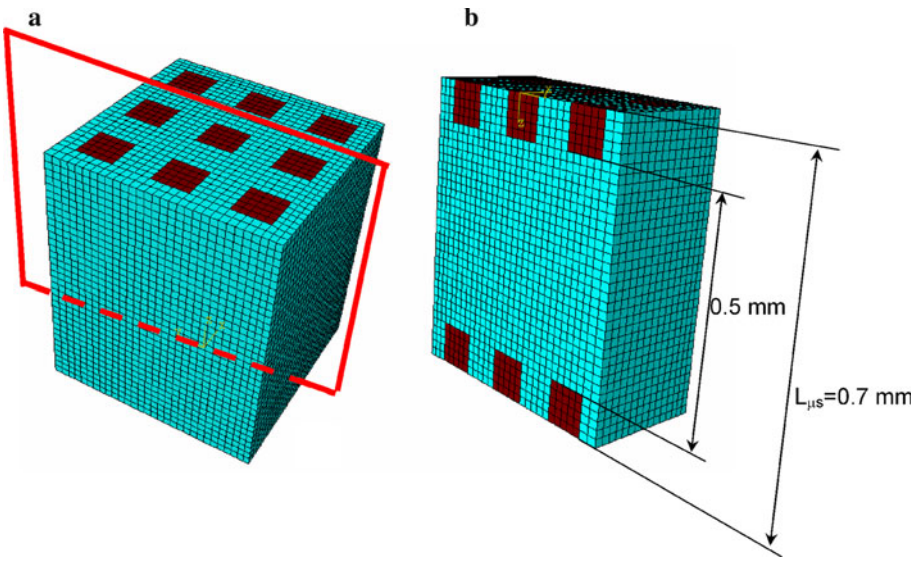

Fig. 3 Geometry (**a**) and section (**b**) of the micro-scale model. In red are represented the trabeculae spicules, in blue sky the granulation tissue (colour figure online)

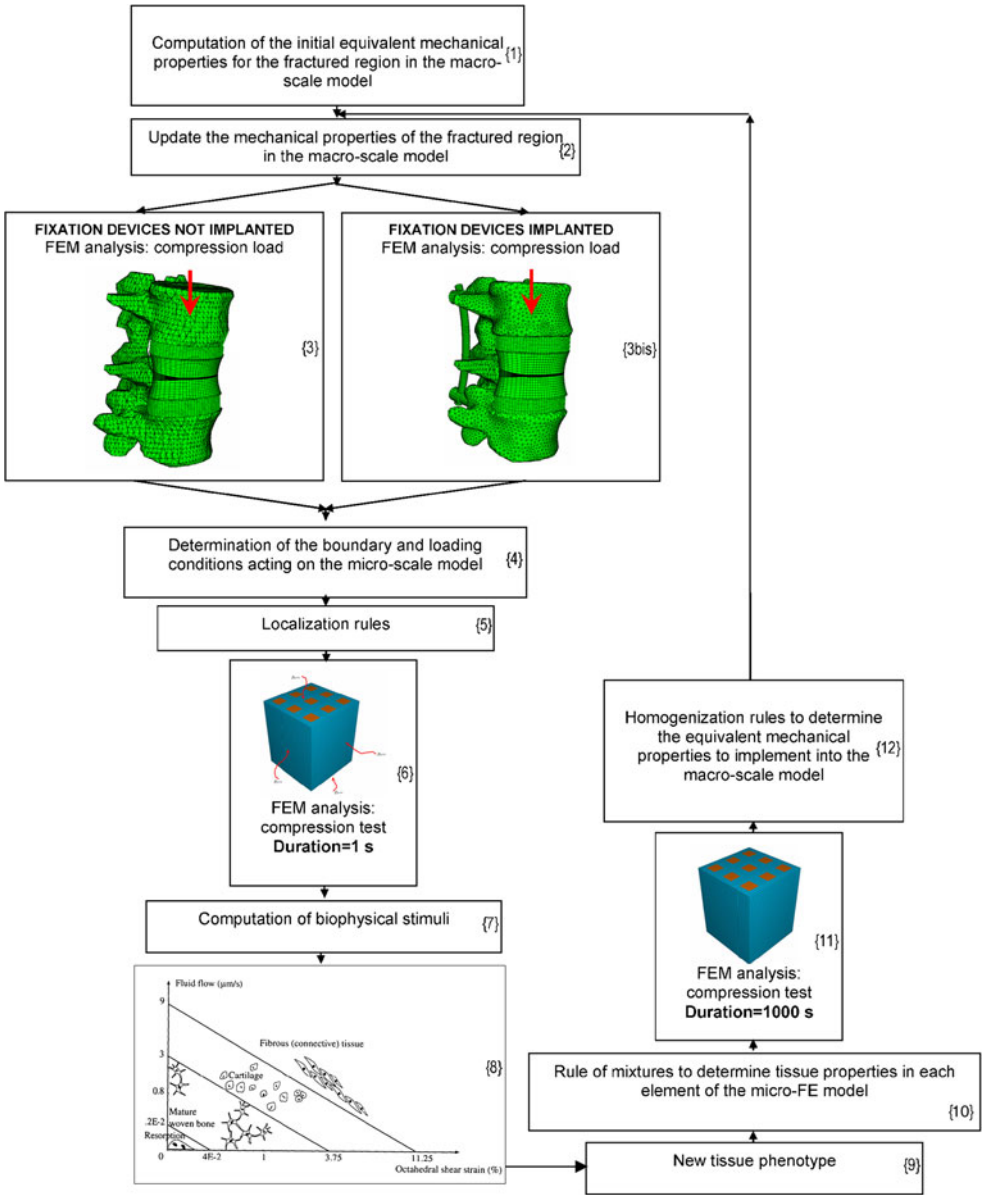

Fig. 4 Schematic of the algorithm utilised to model the fracture repair process both, in the presence and in the absence of fixation devices

conditions as those determined from the macro-scale model (Fig. 4, Block{6}). Following the hypothesis that the inferior surface is constrained, a vertical displacement ΔL_{Pi} is applied on the top surface given by $\Delta L_{\mathrm{Pi}} = \varepsilon_{\mathrm{zzPi}} \times L_{\mu\mathrm{s}}$, $L_{\mu\mathrm{s}} = 0.7$ mm (Fig. 3) being the height of the micro-scale model. The pore pressure averaged on the neighbourhood of each point $P_1, \ldots, P_8$, is applied on the six external faces of each of the eight micro-scale models. The results obtained from this finite element analysis were used to determine the biophysical stimulus acting in each element of the micro-scale model. The biophysical stimulus, according to Huiskes et al. [18], was hypothesised to be a function of the tissue octahedral shear strain and the interstitial fluid flow (note: the trabecular bone and the tissues differentiating in the micro-scale model have been modelled as biphasic poroelastic materials) (Fig. 4, Block{7}). At this point, based on the boundaries of the mechano-regulation diagram proposed by Lacroix and Prendergast [23], the new tissue phenotype was determined for each element of the micro-scale model (Fig. 4, Block{8}, {9}). The elastic modulus of the differentiating tissues can then be estimated according to an exponential law developed previously [5, 6], incorporating a simple rule of mixtures described in Lacroix and Prendergast [23] (Fig. 4, Block{10}). The change of the tissue phenotype leads to a change of the equivalent mechanical properties within the fracture gap of the macro-scale model. In order to determine these equivalent mechanical properties, a new

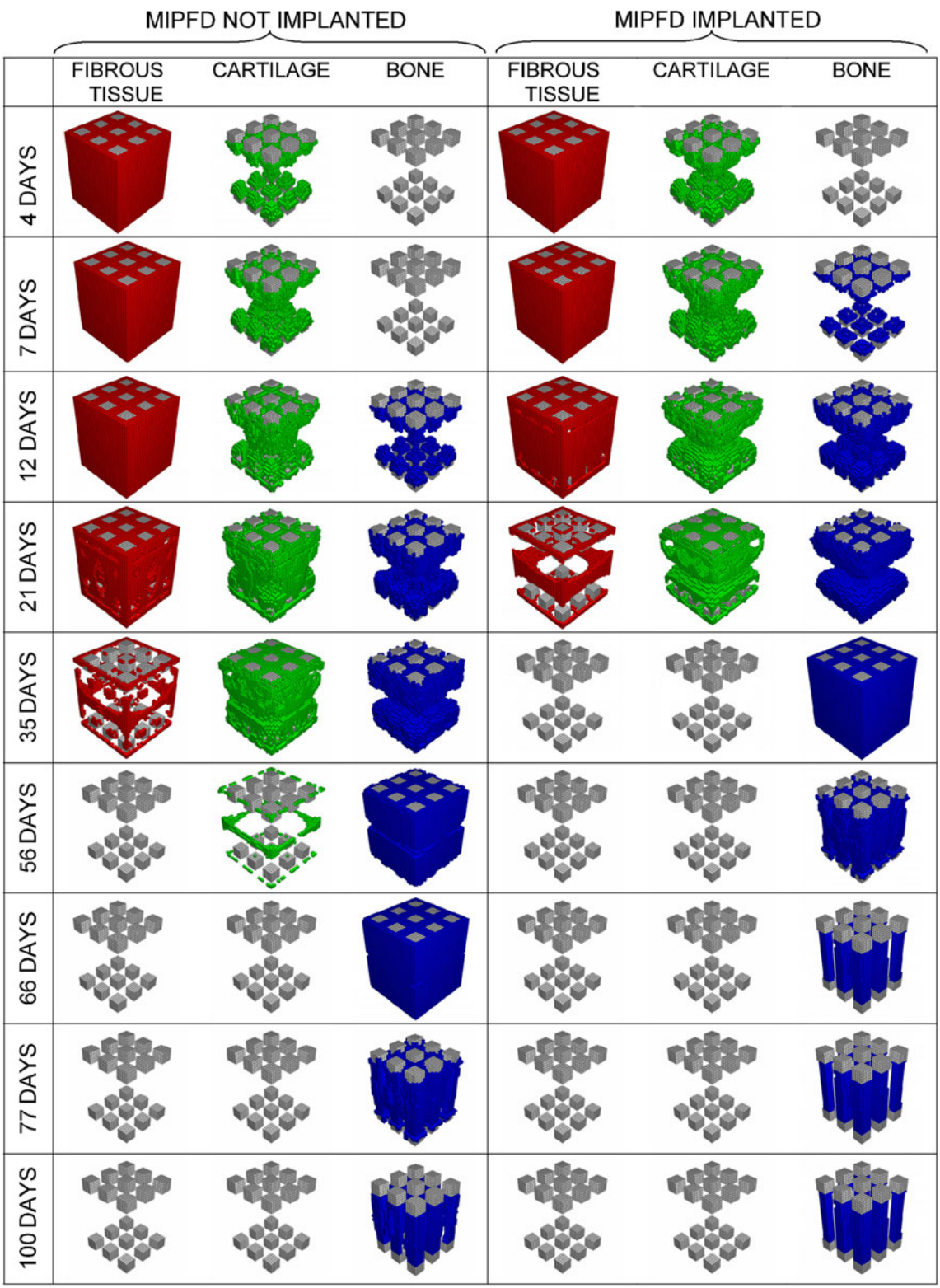

Fig. 5 Patterns of the tissues differentiating during the fracture healing process in the point P_1 in the presence (Cobalt Chrome alloy, $R = 90$ mm, $D = 5.5$ mm) and in the absence of fixation device

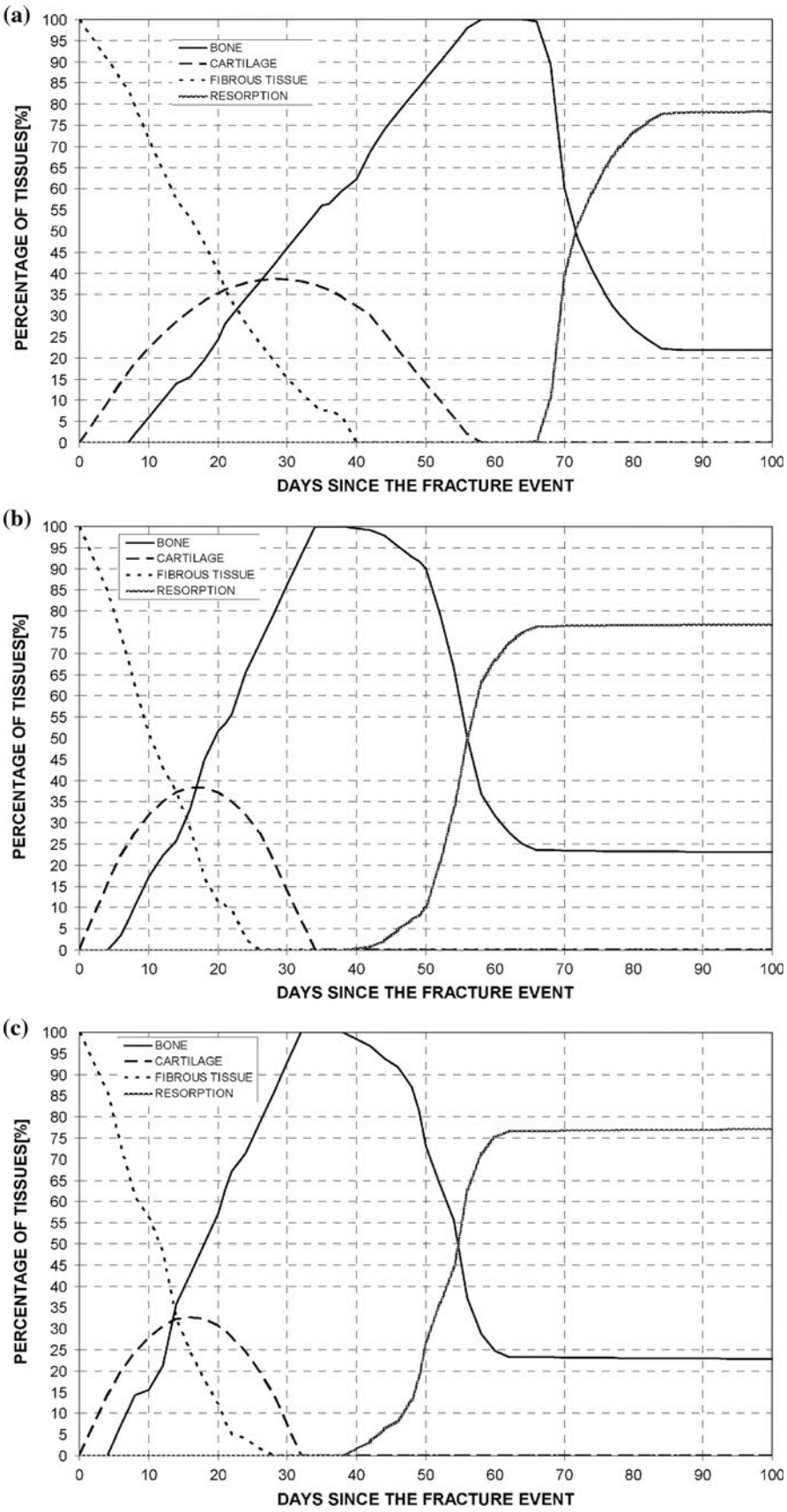

Fig. 6 Percentages of tissues differentiating during the healing process in the point P_1 without **a** and with MIPFD (Ti-6Al-4V alloy, $R = 90$ mm, $D = 5.5$ mm, **b**, Chrome Cobalt, $R = 90$ mm, $D = 5.5$ mm, **c**). The percentages of tissues within the fracture gap have been computed by dividing the number of elements of a given tissue by the total number of elements making up the micro-scale model. 'Resorption' indicates the number of elements for which $S < 0.01$. (Note: The space originally occupied by the trabeculae before the fracture is 1/4 (25 %) of the total available space)

compression test was simulated on the micro-scale geometry (Fig. 4, Block{11}). A displacement δ producing an average strain $\varepsilon_{imp} = 5\ \%$, $\delta = \varepsilon_{imp}\ L_{\mu s}$, is applied on the top surface of the prismatic domain, ramped over a time period of 1,000 s; the inferior surface was hypothesised to be constrained. For such a long time period, the drained condition is reached and then the bone callus, modelled as a biphasic poroelastic material, behaves as an elastic one. Equivalent mechanical properties are determined for each of the eight micro-scale models associated with the points P_1, …, P_8. Knowing the reaction force F at the constraints, the equivalent Young's modulus E_{equiv_ms} (to be implemented into the macro-scale model at the next iteration) is determined as: $E_{equiv\_ms} = \frac{F \times L_{\mu s}}{A \times \delta}$, where A is the transverse section of the micro-scale model. Concerning the other mechanical properties (e.g. Poisson's ratio, etc.), their equivalent value for the macro-scale model was computed as the average of the values of the mechanical properties of each element making up the micro-scale model. Proper homogenization techniques have been finally adopted to switch from the micro- to the macro-scale model (Fig. 4, Block{12}). It was supposed that the spatial changes in the mechanical properties in the macro-scale model could be described with a cubic interpolation law. The variability of the mechanical properties was modelled by means of the user-defined FORTRAN subroutine *UFIELD* available in ABAQUS. Given that only an axial load was applied to the centre of mass of the L3 vertebra, it was assumed that the distribution of the mechanical properties within the vertebral fracture was symmetric with respect to the axis connecting the points P_2 and P_3 and does not change with respect to z (Fig. 1h). The equation describing the change in space of the mechanical properties was of the form:

$$MP = Ax^3 + By^3 + Cx^2y + Dxy^2 + Exy + Fx + Gy + H \quad (1)$$

where MP was the mechanical property under consideration (e.g. Young's modulus, etc.), x and y are the plane coordinates (Fig. 1h). A, B, …., H are eight coefficients computed in each cycle of the algorithm that regulate the shape of the cubic surface MP = MP(x, y) and that are determined by utilising the equivalent mechanical properties computed in each of the eight points P_1, P_2, …, P_8. Further details regarding the algorithm are reported [9].

3 Results

In either the presence or the absence of MIPFD (Fig. 5), the bone repair process is predicted to follow a similar pathway with significant temporal differences. Bone initially forms at the fractured trabecular ends, replacing a cartilaginous template through the process of endochondral bone formation. Then, bone resorption leads to rapid reorganisation of the repair tissue thus favouring the formation of bony bridges linking the trabeculae spicules.

In both the presence and absence of the device, the space between the fractured trabeculae is predicted to be mostly occupied by fibrous tissue in the first days after the fracture event (see Fig. 5 that shows the patterns of tissues predicted for the point P_1). In the absence of a MIPFD, fibrous tissue only disappears completely after 6 weeks (Fig. 6a), while in the presence of a MIPFD, fibrous tissue was predicted to disappear after 4 weeks (Fig. 6b, c). Cartilaginous tissue was predicted to be completely replaced by bone after 2 months in the absence of a MIPFD (Fig. 6a). This process of endochondral ossification was accelerated in the presence of the MIPFD (Fig. 6b, c). After the first month, the space between the fractured trabeculae is entirely occupied by bone if a MIPFD is implanted. Without the support of a MIPFD, the bone remodelling process starts after the second month and is predicted to reach equilibrium at the 85th day, while after implantation of the device the process starts after the first month and reaches equilibrium after about 65 days.

The duration of the healing period—defined as the number of days necessary to have 30 % of the available space occupied by remodelled bony tissue—(Fig. 7a) decreases significantly when a fixation device is implanted (Fig. 7). Also, shorter healing periods are predicted for increasing values of the rod diameter D (for a fixed radius of curvature R) and for decreasing radii of curvature R (for a fixed rod diameter D) (Fig. 7b, c). Finally, the greater stiffness of the cobalt chrome rods allows slightly faster (than those predicted for the Ti-6Al-4V alloy rods) healing processes to occur (Fig. 7b, c).

The maximum value of the von Mises stresses within the device and computed at the end of the healing process was predicted to be localized in correspondence of the point where the rod is attached to the screw (Fig. 8a). The predicted magnitude of stress is sensitive to both the rod diameter D and the radius of curvature R. For increasing rod diameters D (for a fixed radius of curvature R) and radii of curvature R (for a fixed rod diameter D), smaller values of the maximum von Mises stress are calculated (Fig. 8b, c). The predicted maximum von Mises stress is more sensitive to changes in the material with which the rods are realised. In the case of the cobalt chrome alloy, the model computes values of the maximum von Mises stress that are about 1.5 times higher than those predicted in the case of the Ti-6Al-4V alloy.

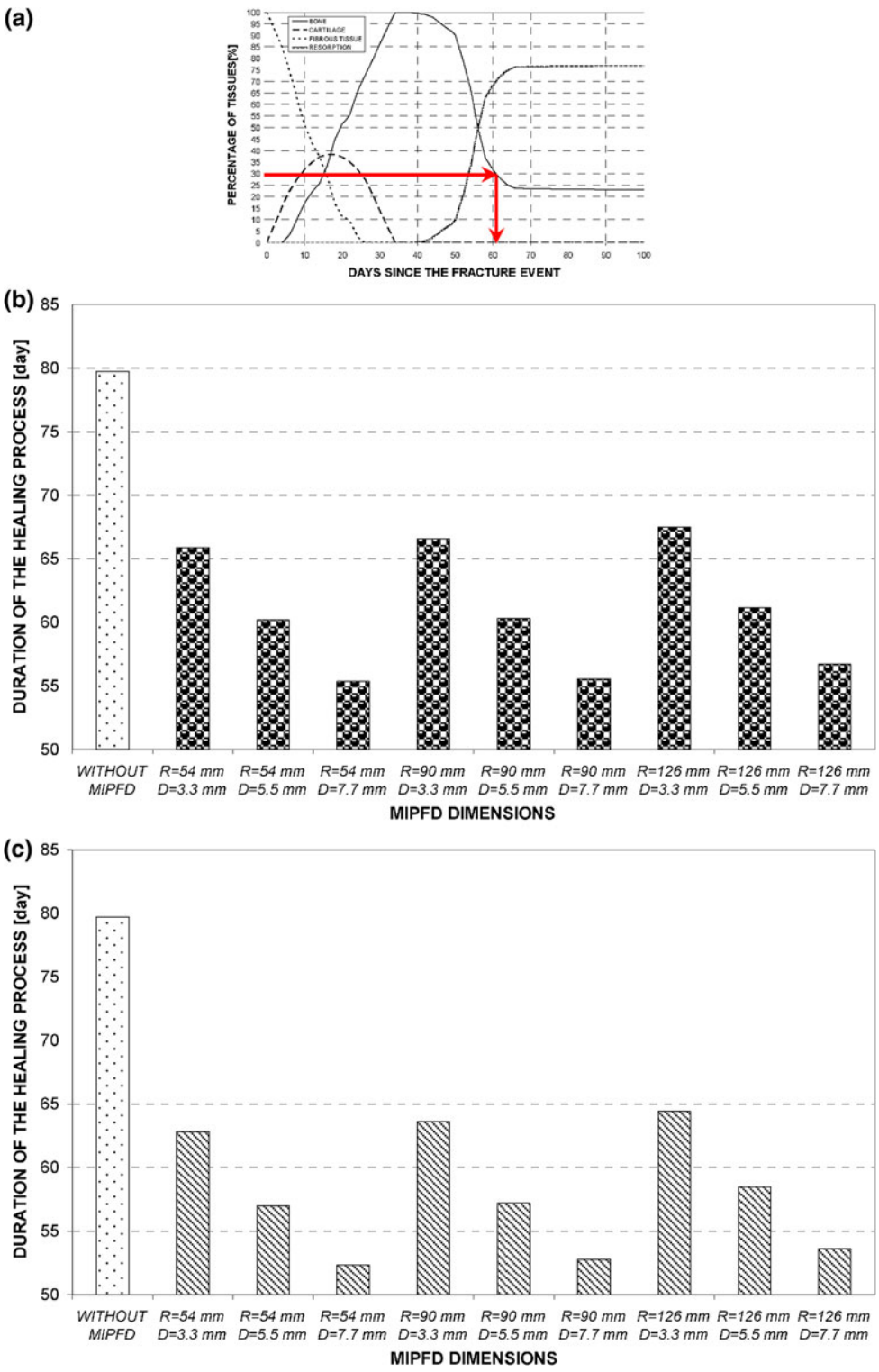

Fig. 7 Duration of the healing process predicted by the numerical model for the different investigated dimensions and for the different materials hypothesised: **b** Ti-6Al-4V alloy, **c** cobalt chrome alloy. The duration has been determined by evaluating the number of days necessary to have 30 % of the available space occupied by remodelled bony tissue (**a**)

4 Discussion

This paper presents a multi-scale mechano-regulation model of a vertebral fracture treated with minimally invasive percutaneous fixation.

The present study has a number of limitations. The mechano-regulation algorithm does not include a damaged tissue region that would allow tissue to fracture and a new callus to form in regions experiencing high levels of bio-physical stimulus [35]. Other factors, such as angiogenesis

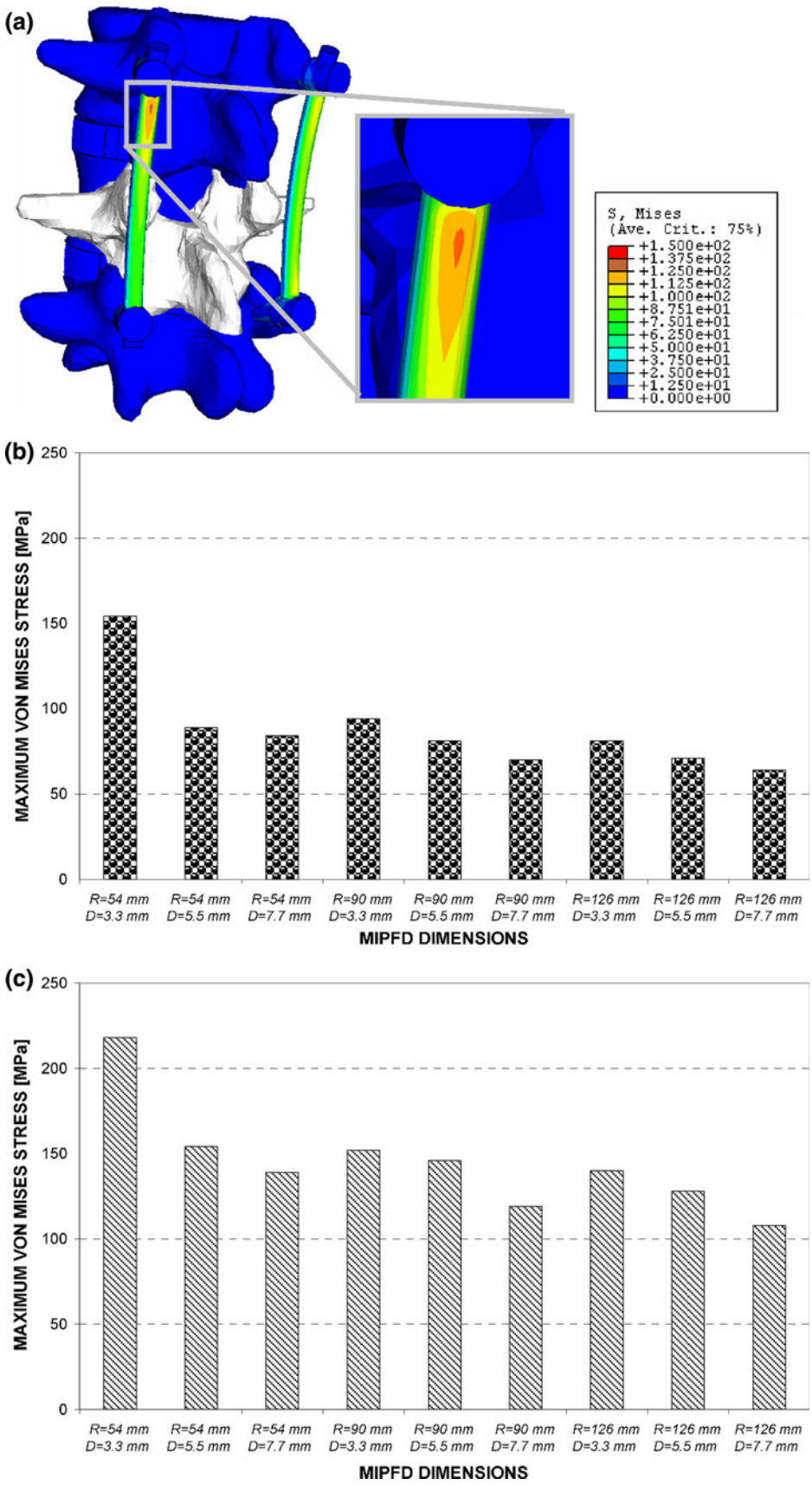

Fig. 8 The maximum values of the von Mises stresses predicted by the model at the 100th day after the fracture event have been found in proximity of the point where the rod is attached to the screw (**a**). Maximum von Mises stresses predicted for the Ti-6Al-4V (**b**) and cobalt chrome alloy (**c**)

[11, 16, 30, 33] and growth factors [2] that could play an important role in fracture healing, were also not included in the model. A simplified micro-scale model of the fractured cancellous bone has been adopted. A finite element model reconstructed from micro-CT data (see for example, the models developed by Sandino et al. [32, 33]) would mimic more accurately the actual morphology of the trabecular vertebral bone. Ideally, the micro-scale analysis should be performed at all the points in the fracture gap. The decision not to perform this at all point was made due to the high computational cost of such an undertaking. We estimate that even using multiple processors this analysis would take years to complete using the available computing resources. Therefore, the choice of eight points (the same number of points was used in our previous study [9]) was the result of a compromise between the accuracy of the obtained results and the computational cost of the analysis. In spite of these limitations, the spatial and temporal patterns of tissue differentiation predicted by this model in the absence of a device are in general agreement [9] with those observed experimentally [15]. Diamond et al. [15] describe four stages of fracture healing process in the vertebral body: (i) fracture haematoma, (ii) chondrogenesis and bone matrix synthesis, (iii) endochondral ossification and woven bone formation, and (iv) bone modelling and remodeling. The same stages of fracture healing process are predicted by the present model in the absence of a fixation device at comparable time points [9]. Currently, to the knowledge of the present authors, no data are reported in the literature describing the patterns of tissue differentiation observed in vertebral fractures treated with fixation devices. The model predicts that use of fixation devices allows the healing times to be significantly shortened (Figs. 5, 6, 7, 8), which has also been described in the literature [3, 27].

By increasing the global stiffness of the L3-L4-L5 spinal segment, the device decreases the average value of the biophysical stimulus acting on the mesenchymal tissue thus allowing a faster formation of bony tissue and subsequent remodeling. The higher stiffness of the cobalt chrome alloy with respect to that exhibited by the Ti-6Al-4V alloy was also predicted to reduce displacements in the fracture gap of the macro-scale model thus reducing the level of strain (i.e. the biophysical stimulus) in the mesenchymal tissue.

The model predicted that increasing the rod diameter D and decreasing the radius of curvature R shortens the healing period. However, the healing period appears to be more sensitive to the rod diameter rather than to the radius of curvature (Fig. 7b, c). While it is intuitive that increasing values of the rod diameter will lead to greater stability and hence a prediction of a shorter duration of the healing process, less obvious is the reason for the prediction of accelerated healing with decreasing values of the radius of curvature. To understand this finding, consider a single device for fixation schematized as the combination of two straight beams and a curved one (Fig. ESM_2a available online (ESM_2.pdf)). The straight beams represent the screws while the curved beam represents the rod. The displacement δ of the point G along the vertical direction can be determined by applying Castigliano's theorem. If Q is the load applied at the point G, the stiffness K_G can defined as: $K_G = Q/\delta$. Assuming that the effect of the normal and the shear stress is negligible, one can express the stiffness K_G in function of the radius of curvature R (Fig. ESM_2b available online (ESM_2.pdf)). Appendix A, available online (ESM_2.pdf), illustrates the mathematical formulation adopted to determine $K_G = K_G(R)$. The continuous line refers to the case chrome cobalt alloy ($E_R = 230{,}000$ MPa, $\nu = 0.3$), while the dashed line refers to the case Ti-6Al-4V alloy ($E_R = 110{,}000$ MPa, $\nu = 0.3$) (Fig. ESM_2b). It can be seen that as we move towards increasing radii of curvature R, decreasing values of K_G, or, equivalently, increasing values of δ are predicted. This explains why the proposed mechano-regulation model predicts longer durations of the healing period for increasing radii of curvature. These results would push the surgeon to use smaller radii of curvature; however, such a choice would lead to higher values of the maximum von Mises stresses within the device (Fig. 8).

The von Mises stress values predicted (after 100 days since the fracture event) in the cobalt chrome alloy rods are higher than those predicted for the Ti-6Al-4V rods (Fig. 8). The peak stresses are well below the fatigue limit (for the Ti-6Al-4V alloy, $\Delta\sigma_{LIM} = 510$ MPa; for the cobalt chrome alloy $\Delta\sigma_{LIM} = 610$ MPa) for both the alloys. This allows us to conclude that for the hypothesised load acting on the lumbar segment the risk of failure of the fixation device is low. In clinical practice, when fixation involves the L2 or lower segments, due to the possible risk of failure, the device is removed [27]. The removal typically occurs after 10–12 months since the surgical treatment; at this time, the healing process practically has terminated and then the lumbar segment L3-L4-L5 can be subjected not only to compression load (i.e. the load hypothesised in this study) but also to a combination of compression load and flexion–extension, axial and lateral-flexion moment which certainly induce local peaks of stress greater than those induced within the device with the sole compression load. These stresses can also assume high values in view of the significant mobility of the spine at the lumbar level and can lead, after a given number of loading cycles to failure of the device. Interestingly, predicted von Mises stress peaks are of the same order of magnitude as those determined numerically by Kim and Kim [22] although the model presented by these authors refers to a different spinal device that only approximately reproduces the geometry of the fixation device investigated in the present study.

In conclusion, in this paper, using a mechano-regulation model, the process of tissue differentiation and bone remodelling in a vertebral fracture treated with a fixation device has been simulated. Different geometrical dimensions have been investigated for the individual components of the device. In addition, the effect of the mechanical properties of the material with which the rod component can be realised has also been investigated. The Von Mises stress distribution was determined within the fixation device for assessing the possible risk of its failure and for understanding if its removal is required. Analyses revealed that the dimension of the screw diameter has negligible effects on the predicted patterns of tissue differentiation. More interesting appeared the effects of the rod diameter D as well as of its radius of curvature R. Increasing values of D and decreasing values of R lead to predictions of shorter durations of the healing period. However, for decreasing values of R, if D remains constant, higher von Mises stress peaks are predicted. Finally, the analyses carried out revealed that realising the rods in cobalt chrome alloy allows slightly shorter healing periods to be obtained (with respect to the case of rods in Ti-6al-4V) as well as heavier loads to be applied on the spinal segment.

The computational model presented in this paper seems to be a promising tool able to predict how the choice of the different components of the fixation device and the modalities with which the device is implanted on the fractured spinal segment can affect the outcome of the healing process.

References

1. Ament C, Hofer, EP (2000) A fuzzy logic model of fracture healing. J Biomech 33:961–918
2. Bailón-Plaza A, van der Meulen MCH (2001) A mathematical framework to study the effects of growth factor influences on fracture healing. J Theor Biol 212:191–209
3. Barbanti Brodano G, De Iure F, Cappuccio M, Palmisani M, Boriani L, Gasbarrini A, Bandiera S, Scimeca GB, Boriani S (2007) Osteosintesi con tecnica percutanea mininvasiva nel trattamento delle fratture vertebrali toraciche e lombari. Esperienza preliminare. Giornale Italiano di Ortopedia e Traumatol (GIOT) 33:78–85 (publication in Italian)
4. Been HD, Poolman RW, Ubags LH (2004) Clinical outcome and radiographic results after surgical treatment of post-traumatic thoracolumbar kyphosis following simple type A fractures. Eur Spine J 13:101–107
5. Boccaccio A, Pappalettere C, Kelly DJ (2007) The influence of expansion rates on mandibular distraction osteogenesis: a computational analysis. Ann Biomed Eng 35:1940–1960
6. Boccaccio A, Prendergast PJ, Pappalettere C, Kelly DJ (2008) Tissue differentiation and bone regeneration in an osteotomized mandible: a computational analysis of the latency period. Med Biol Eng Comput 46:283–298
7. Boccaccio A, Vena P, Gastaldi D, Franzoso G, Pietrabissa R, Pappalettere C (2008) Finite element analysis in cancellous bone failure in the vertebral body of healthy and osteoporotic subjects. Proc Inst Mech Eng H 222:1023–1036
8. Boccaccio A, Ballini A, Pappalettere C, Tullo D, Cantore S, Desiate A (2011) Finite element method (FEM), mechanobiology and biomimetic scaffolds in bone tissue engineering. Int J Biol Sci 7:112–132
9. Boccaccio A, Kelly DJ, Pappalettere C (2011) A mechano-regulation model of fracture repair in vertebral bodies. J Orthop Res 29:433–443
10. Carter DR, Blenman PR, Beaupré GS (1988) Correlations between mechanical stress history and tissue differentiation in initial fracture healing. J Orthop Res 6:736–748
11. Checa S, Prendergast PJ (2009) A mechanobiological model for tissue differentiation that includes angiogenesis: a lattice-based modeling approach. Ann Biomed Eng 37:129–145
12. Chow GH, Nelson BJ, Gebhard JS, Brugman JL, Brown CW, Donaldson DH (1996) Functional outcome of thoracolumbar burst fractures managed with hyperextension casting or bracing and early mobilization. Spine 21:2170–2175
13. Claes LE, Heigele CA, Neidlinger-Wilke C, Kaspar D, Seidl W, Margevicius KJ, Augat P (1998) Effects of mechanical factors on the fracture healing process. Clin Orthop Relat Res 355(suppl):S132–S147
14. Claes LE, Heigele CA (1999) Magnitudes of local stress and strain along bony surfaces predict the course and type of fracture healing. J Biomech 32:255–266
15. Diamond TH, Clark WA, Kumar SV (2007) Histomorphometric analysis of fracture healing cascade in acute osteoporotic vertebral body fractures. Bone 40:775–780
16. Geris L, Gerisch A, Sloten JV, Weiner R, Oosterwyck HV (2008) Angiogenesis in bone fracture healing: a bioregulatory model. J Theor Biol 251:137–158
17. Gòmez-Benito MJ, Garcìa-Aznar JM, Kuiper JH, Doblaré M (2005) Influence of fracture gap size on the pattern of long bone healing: a computational study. J Theor Biol 235:105–119
18. Huiskes R, van Driel WD, Prendergast PJ, Søballe K (1997) A biomechanical regulatory model of periprosthetic tissue differentiation. J Mater Sci Mater Med 8:785–788
19. Isaksson H, Wilson W, van Donkellaar CC, Huiskes R, Ito K (2006) Comparison of biophysical stimuli for mechano-regulation of tissue differentiation during fracture healing. J Biomech 39:1507–1516
20. Isaksson H, van Donkelaar CC, Huiskes R (2008) A mechano-regulatory bone-healing model incorporating cell-phenotype specific activity. J Theor Biol 252:230–246
21. Kelly DJ, Prendergast PJ (2005) Mechano-regulation of stem cell differentiation and tissue regeneration in osteochondral defects. J Biomech 38:1413–1422
22. Kim Y, Kim TW (2010) Finite element analysis of the effects of pedicle screw fixation nut loosening on lumbar interbody fusion based on the elasto-plateau plasticity of bone characteristics. Spine 35:1–8
23. Lacroix D, Prendergast PJ (2002) A mechano-regulation model for tissue differentiation during fracture healing: analysis of gap size and loading. J Biomech 35:1163–1171
24. Mizrahi J, Silve MJ, Keaveny TM, Edwards WT, Hayes WC (1993) Finite-element stress analysis of the normal and osteoporotic lumbar vertebral body. Spine 18:2088–2096
25. Mumford J, Weinstein JN, Spratt KF, Goel VK (1993) Thoracolumbar burst fractures. The clinical efficacy and outcome of nonoperative management. Spine 18:955–970
26. Nagel T, Kelly DJ (2010) Mechano-regulation of mesenchymal stem cell differentiation and collagen organisation during skeletal tissue repair. Biomech Model Mechanobiol 9:359–372
27. Palmisani M, Gasbarrini A, Barbanti Brodano G, De Iure F, Cappuccio M, Boriani L, Amendola L, Boriani S (2009)

Minimally invasive percutaneous fixation in the treatment of thoracic and lumbar spine fractures. Eur Spine J 18:S71–S74
28. Pape HC, Giannoudis P, Krettek C (2002) The timing of fracture treatment in polytrauma patients: relevance of damage control orthopedic surgery. Am J Surg 183:622–629
29. Pauwels F (1980) A new theory concerning the influence of mechanical stimuli on the differentiation of the supporting tissues. In: Maquet P, Furlong R (eds) Biomechanics of the locomotor apparatus. Springer, Berlin, pp 375–407
30. Peiffer V, Gerisch A, Vandepitte D, Van Oosterwyck H, Geris L (2011) A hybrid bioregulatory model of angiogenesis during bone fracture healing. Biomech Model Mechanobiol 10:383–395
31. Pérez MA, Prendergast PJ (2007) Random-walk models of cell dispersal included in mechanobiological simulations of tissue differentiation. J Biomech 40:2244–2253
32. Sandino C, Planell JA, Lacroix D (2008) A finite element study of mechanical stimuli in scaffolds for bone tissue engineering. J Biomech 41:1005–1014
33. Sandino C, Checa S, Prendergast PJ, Lacroix D (2010) Simulation of angiogenesis and cell differentiation in a CaP scaffold subjected to compressive strains using a lattice modeling approach. Biomaterials 31:2446–2452
34. Seybold EA, Sweeney CA, Fredrickson BE, Warhold LG, Bernini PM (1999) Functional outcome of low lumbar burst fractures. A multicenter review of operative and nonoperative treatment of L3–L5. Spine 24:2154–2161
35. Shefelbine SJ, Augat P, Claes L, Simon U (2005) Trabecular bone fracture healing simulation with finite element analysis and fuzzy logic. J Biomech 38:2440–2450
36. Shen WJ, Shen YS (1999) Nonsurgical treatment of three-column thoracolumbar junction burst fractures without neurologic deficit. Spine 24:412–415
37. Shen WJ, Liu TJ, Shen YS (2001) Nonoperative treatment versus posterior fixation for thoracolumbar junction burst fractures without neurologic deficit. Spine 26:1038–1045
38. Simon U, Augat P, Utz M, Claes L (2003) Simulation of tissue development and vascularisation in the callus healing process. In: Transactions of 49th annual meeting orthopaedic research society, New Orleans
39. Wang ST, Ma HL, Liu CL, Yu WK, Chang MC, Chen TH (2006) Is fusion necessary for surgically treated burst fractures of the thoracolumbar and lumbar spine? A prospective, randomized study. Spine 31:2646–2652
40. Wood K, Buttermann G, Mehbod A, Garvey T, Jhanjee R, Sechriest V (2003) Operative compared with nonoperative treatment of a thoracolumbar burst fracture without neurological deficit. A prospective, randomized study. J Bone Jt Surg Am 85(A):773–781